# Rolling Bearing Fault Detection Based on Vibration Signal Analysis and Cumulative Sum Control Chart

**Saja Mohammed Jawad**
MS.c Student
Mechanical Engineering Department
University of Technology
Iraq

**Alaa Abdulhady Jaber**
Assistant Professor
Mechanical Engineering Department
University of Technology
Iraq

*Monitoring the condition of rotating machines is essential for the systems' safety, reducing maintenance costs, and increasing reliability. In this research, a fault detection system for bearings was developed using the vibration analysis technique with the statistical control chart approach. A test rig was first designed and constructed; then, various bearing faults, such as inner race and outer race faults, were simulated and examined in the test rig. After capturing the vibration signals at different bearing health conditions, the time-domain signal analysis technique was employed for extracting different indicative features.The obtained time domain features were then analyzed to find out the most fault-significant feature. Then, only one feature was selected to design the control chart for bearing health condition monitoring. The cumulative sum control chart (CUSUM was utilized since it can detect the small changes in bearing health states. The results showed the effectiveness of utilizing this method, and it was found that the percentage of the out-of-control points in the event of the combined cage and ball fault to the number of tested samples is greater than the other fault types.*

***Keywords:*** *CUSUMChart; Statistical Control Chart; Vibration Analysis; Rolling Bearing Health Monitoring, Fault Detection*

## 1. INTRODUCTION

Rotating machinesare important for different industries, such as oil and gas industries, construction, and power plant industries.A catastrophic failure of rotating machinery would have a huge effect on the manu–facturing sector. As the malfunction progresses, the machine's energy consumption will increase, while its performance will decrease.Gradually, followed by a sudden failure, will not only decrease production vo–lume but will also result in increased operating costs for the reconstruction, as well as wasting time for the employees as they wait.On a larger scale, continued use of a defective machine could result in physical injury to the person operating the machine, and in the worst-case scenario, death [1]. A rolling bearing part is a critical com–ponent in engineering machinery, and even minor damage can result in unexpected production halts or industrial accidents.Bearing faults can occur for various reasons, including heavy loads that are unstable and inadequate lubrication[2]. As a result, early identifi-cation and diagnosis of faults will greatly reduce the im-pact of defective machinery. It is highly cost-effective, reducing output losses and increasing productivity while also improving human and environmental protection[1]. Acoustic analysis, temperature control, oil analysis, stator current, and vibration analysis can all be used to detect bearing defects[3]. While vibration analysis is better for detecting mechanical faults, current analysis can also be used to detect mechanical defects because induction motor current consumption is changed by mechanical efforts and vibrational patterns in rotating machines. The use of acoustic emission signals is the subject of sound analysis[4]. Analysis of vibrations helps track the machine's operating conditions and compare them based on the analysis results in normal operating conditions to see if there is a problem. This will help prevent disasters and identify faults early on. The vibration control theory is that all devices generate vibration, but the vibration is relatively small when the machine/works under normal operating conditions, but the vibration amplitude changes when a malfunction occurs[5].

Vibration analysis is necessary for analyzing structures and preventing failure. It contains information about the structure'smode shapes and natural frequencies, which are widely used for fault detection purposes[6-8].Time-domain and frequency-domain vibration techniques are used separately or in combination for bearing performance analysis. Features such as Root Mean Square, Crest Factor, Kurtosis, and others are used in the time-domain analysis, whereas the Fourier Transform technique is used in the frequency-domain analysis [9].Also, control charts are a good example of a statistical process control system.The Shewhart X map is widely used for mean shift detection due to its ease of use.The exponentially weighted moving average (EWMA) and cumulative sum (CUSUM) graphs are commonly used to detect relatively minor changes. For detecting divergence shifts, the standard deviation (S) and range (R) charts are useful[10]. As a result, combining the statistical

Received: May 2021, Accepted: June 2021
Correspondence to: Alaa Abdulhady Jaber, Assistant Professor, Mechanical Engineering Department, University of Technology, Baghdad, Iraq
E-mail: Alaa.A.Jaber@uotechnology.edu.iq
**doi:10.5937/fme2103684M**

control chart with artificial intelligence techniques may result in a reliable machinery health monitoring system that can simultaneously detect and diagnose various fault forms[11].

Therefore, this paper aims to develop a health monitoring system to detect and diagnose the most common bearing faults using vibration analysis technology and statistical control diagram approach. To achieve this, a critical review was conducted of recent and previous research in bearing health monitoring, designing, and manufacturing a test platform to conduct the required experimental work. After that, a suitable system for data acquisition, signal analysis, and feature extraction was developed, and then an appropriate control scheme was designed to detect the bearing faults.

This paper isorganized as follows: The second section contains the theoretical aspects behind the vibration analysis method, such as the time domain and frequency signal analysis, and discusses the theory of statistical control charts.In the third section, the design and development of the proposed test rigareprovided. The developed data acquisition system based on the LabVIEW software was also discussed. Section four shows the obtained results of this study, including a discussion of the most important findings. It also discusses the method for selecting the appropriate feature for designing and testing the control scheme. Finally, the paper is wrapped up in the conclusion section, which highlights the main obtained findings.

## 2. THEORETICAL FOUNDATIONS OF THE ANALYSIS

### 2.1 Vibration Measurement Techniques

Since it is accurate and sensitive to fault intensity, vibration monitoring is the most useful technique. Because of varying compliance or defects in bearing components, bearings serve as a source of vibration and noise. These vibration signals will provide us with details on the bearing's state [12].Therefore, the most common method for diagnosing rolling element bearing faults is vibration monitoring. The commonly followed vibration signal analysis techniques can mainly be categorized into time-domain, frequency-domain, and time-frequency domain.

### 2.2 Time domain technique Analysis

In general, time-domain analysis is used to track the condition of bearings. Root mean square, kurtosis, crest factor, skewness, and peak-to-peak are some of the statistical parameters utilized in time domain analysis to monitor the health of bearings[13]. The feature that is selected has a significant effect on pattern recognition performance. To detect initial bearing damage, the above mentioned time-domain statistical parameters are calculated as in the following:

**Peak value ($P_v$)**: It denotes the maximum value of the amplitude of the information set. Mathematically, it is calculated based on the following equation[3]:

$$P_v = (1/2)\left[\max(x_i) - \min(x_i)\right] \tag{1}$$

where $x_i$ ($i = 1, ...,N$) is the amplitude at a sampling point*i*and N is the number of sampling points [14].

**Root Mean Square (RMS):**The RMS is a feature that measures the power content in the vibration signature. This feature is very effective when detecting an imbalance in rotating machinery. The most basic approach to measuring defects in the time domain is to utilize the RMS approach, which is often not sensitive enough to detect fault initiation[15].

$$RMS = \sqrt{\frac{1}{N}\sum_{i=1}^{N}(X_i)^2} \tag{2}$$

**Standard deviation:**The standard deviation display the dispersion of a collection of data with respect to the mean, and its magnitude equals the variance's arithmetic mean value[2] can be calculated by the following equation:

$$SD = \sqrt{\frac{1}{N}\sum_{i=1}^{N}(X_i - \bar{X})^2} \tag{3}$$

**Kurtosis value:**It is one of the substantial statistical indicators for defect detection in rolling bearings. It is especially beneficial in detecting bearing failure, which compromises measurement between the insensitive lower moments and the over-sensitive higher moments [16].

$$K_v = \frac{\frac{1}{N}\sum_{i=1}^{N}(X_i - \bar{X})^4}{(RMSvalue)^4} \tag{4}$$

**Crest factor:**: It is the ratio of peak value to the RMS value of the signal. It represents how extreme the peaks are in the datasets. The CF near to 1 represents a lower spiky signal. The $C_{rf}$ is calculated based on the fol–lowing equation [3]:

$$C_{rf} = \text{Peak value / RMS value} \tag{5}$$

**Skewness:** It quantifies the asymmetry behavior of vibration signals through its probability density function (PDF). The *Sk* is calculated using Equation 6 below [17].

$$Sk = \frac{1}{N-1}\sum_{i=1}^{N}(X_i - \bar{X})^3 \tag{6}$$

### 2.3 Frequency domain techniques

Frequency domain or spectral analysis technique is the most widely utilized approach for defect diagnosis in bearings. The frequency-domain signal analysis technique converts the time-domain vibration signals into separated frequency components utilizing the fast Fourier transform (FFT) [18, 19]. In the frequency spectrum plot, the X-axis represents the frequency, and the Y-axis represents the amplitude. Therefore, the frequency-domain technique can easily detect certain frequency components, advantageous over the time-domain tech–nique [20].

### 2.4 Time-frequency domain analysis

The signals produced by defective parts are non-stati–onary. If the Fourier transform is used to measure the

frequency variable of non-stationary signals, the results will display the frequency composition averaged over the durationof the signal.As a result, the Fourier transform cannot accurately characterize the charac–teristics of a transient signal; however, because of its ability to represent signals in both the frequency and time domains, time-frequency analysis has been inves-tigated and applied for machinery fault diagnosis. Because of this one-of-a-kind feature, time-frequency analysis techniques are appropriate for non-stationary signals. Furthermore, time-frequency approaches may provide useful information about energy distribution across frequency bands.A variety of time-frequency analysis techniques, such as short-time Fourier trans-form (STFT), wavelet transform (WT), wavelet packet transform (WPT), Hilbert-Huang transform (HHT), etc., have been utilized to identify and diagnose faults [21].

### 2.5 Statistical Control Charting Concept

The control chart is the most significant tool that helps to know whether a process is in control or not. The design of control charts depends firstly on identifying the distribution of the process characteristics followed by monitoring the stability of its parameters. In general, the control chart consists of three important lines: the centerline (CL), the upper control limit (UCL), and the lower control limit (LCL). These limits are selected such that almost all the information will lie between these limits as long as the process remains statistically in control. The power of a control chart is defined as the probability of detecting an out-of-control signal, while the ARL represents the average number of samples wanted to signal an out-of-control situation in the process.

There are three major classifications of charts to monitor the health conditions, namely, Shewhart-type control charts, cumulative sum (CUSUM) charts, and the exponentially weighted moving average (EWMA) charts [22]. The Shewhart-type control charts are highly suitable for detecting large shifts, while CUSUM and EWMA charts are effective for smaller shifts in the parameters of interest. In addition, the CUSUM charts can efficiently address the small shift detection problem [22-24].

### 2.6 Cumulative Sum (Cusum) Charts

CUSUM chart is a graphical method that depends on sequential monitoring of cumulative performance over time, where it depends on sequential procedures and lets timely identification of deterioration in performance [25]. CUSUM control charts were first suggested by Page in 1954 and studied by many authors afterward [26]. This chart relies on current data as the Shewhart control chart and utilizesthe past data to update their plotting statistics. This feature assists the control charts in detecting continuous small and medium shifts in the process parameters [27]. The CUSUM chart plots the cumulative sums of deviations of sample values from the target value.The target value is user-selected. The mean value can be taken for the target value.

There are two general approaches to devising the control limits for the CUSUM control chart. The older method is the V-mask procedure, and the other method is the tabular procedure. The tabular procedure is particularly attractive when the CUSUM is implemented on a computer. So, in this research, the tabular approach is selected to design the CUSUM chart. To apply this method, we need to calculate values $S_H$ and $S_L$, which arethe upper one-sided CUSUM and the lower one-sided CUSUM, respectively.These quantities are calcu-lated from [28]:

$$S_H(i) = \max\left[0, \bar{x}_i - (\mu_0 + K) + S_{H(i-1)}\right] \tag{7}$$

$$S_L(i) = \max\left[0, -\bar{x}_i - (\mu_0 + K) + S_{L(i-1)}\right] \tag{8}$$

where $\bar{x}_i$ is the measured value; the initial values of $S_H$(i) and $S_L$(i) are zeros.K is called the reference value, which is ordinarily selected about halfway between the target $\mu_0$ and the value of the mean corresponding to the out-of-control state $\mu_1 = \mu_0 + \Delta$. This means thatK is about one-half the magnitude of the shift that we are interested in:

$$K = \frac{\delta \times S}{2} \tag{9}$$

where $\delta$ = 0.5, and $S$ is the standard deviation. Hence, the upper control limit (UCL) and lower control limit (LCL) can be calculated using the following equations:

$$UCL = h \times S \tag{10}$$

$$LCL = -h \times S \tag{11}$$

where $h$ is a value usually taken between 4 and 5[29]. Notice that $S_H$(i) and $S_L$(i) accumulate the deviations from the target value greater than $K$, with both quantities reset to zero upon becoming negative. If either $S_H$(i) or $S_L$(i) exceeds the constant UCL or LCL, the process is considered out of control. The interval betweenthe UCL and LCL is usually called the decision interval [29-31].

## 3. EXPERIMENTAL WORK

This section details the experimental work carried out in this study, including the test rig design, fault simulation, data acquisition method, and feature extraction. It discusses the different conducted experiments consi-dering various working conditions on the designed test rig when different bearing faults are simulated.

### 3.1 Test Rig Fabrication

The objective of the fabricated test rig is to create a full-scale platform test rig to conduct the needed tests on the bearings at different health states. The main components of this test rig are the steel frame,1 HP (0.75 kW) AC motor, pulleys (driver fixed on motor and driven fixed on a shaft by key and seal), a belt, and a mild steel shaft of 20 mm diameter mounted on two identical deep groove ball bearings that are fixed in two housing made of cast iron. The details of the used ball bearing are presented in Table 1.

The load was applied using a simple mechanism that makes the bearing housing moving on the frame utilizing

a steel plate (lever) designed to be placed between the bearing housing and the rig's base through a slot on the frame. This mechanism can pull the bearing housing and the shaft with the pulley and the belt, and thus a force will be imposed on the shaft. This force can be changed by changing the pulling forces via the tension rod to easily pulling the system, as shown in Figure 1. To put more flexibility in the developed test rig, a slot was made under the motor to make it easy to move linearly to increase or decrease the load on the shaft [32].

**Table 1: Specification of 6304 ball bearing**

| | |
|---|---|
| Number of balls ($N_b$) | 7 |
| Bore diameter | 20 (mm) |
| Outside diameter | 52 (mm) |
| Bearing contact angle | 0 |

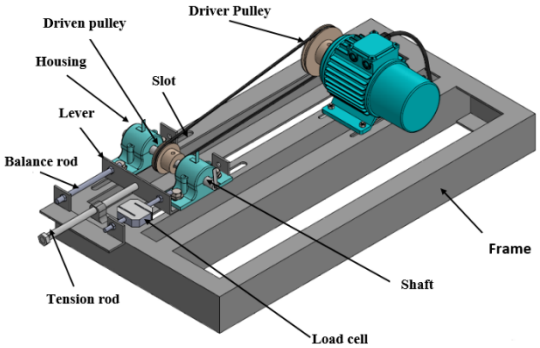


**Figure 1. Solidwork model of the proposed test rig**

Keys were used for fixing the pulleys on the motor's shaft and the bearings' (driven) shaft. A key is a steel part that connects a rotating machine element to its shaft. A key keeps the two pieces from rotating relative to each other, allowing torque transmission to occur. Both the shaft and rotating parts (pulleys) must have a keyway and a keyseat for a key to work effectively. In most cases, a keyseat refers to a groove or pocket on a shaft, while a keyway refers to a slot in a hub where the key fits. A keyed joint is the name given to the entire configuration.Also, to give the structure stability when taking the readings and preventing the generation of unwanted vibrations, a U-section channel of (6 mm) thickness was chosen because it is heavy and stabilizes the structure. In addition, four rubber pieces have been placed under the structure to provide stability to the system. The used induction motor is of fixed speed type; however, to simulate different working speeds on the system, a variable frequency drive (VFD) of type N700E inverter from Hyundai was employed to control the rotation speed.Bearing vibration was measured by fixing a MEMS-type accelerometer on the left bearing using a rectangular steel adapter. The accelerometer was fastened on the adapter using screws. Also, to measure the velocity of the shaft, a laser tachometer was utilized.

### 3.2 Bearing Fault Simulation

Four fault types are simulated in the bearing: inner race fault, outer race fault, combined cage and ball fault and combined inner and outer race fault. The faults are produced using the electrical discharge machining (EDM) technique [33]. The fault's diameter of the outer and inner races was 3.2 mm. This was done using a copper electrode with a diameter of 3.2 mm installed vertically in the machine to make the malfunction on the outer race, while the fault in the inner race was made by turning theelectrode end by an angle of 90, as shown in Figure 2.

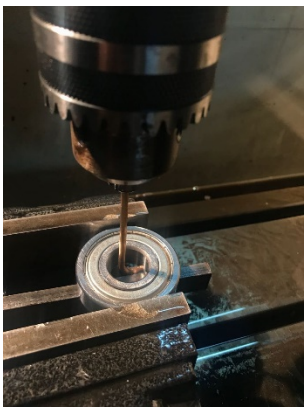

**Figure 2. Inner race fault simulation method**

The purpose of these faults is to investigate the vibration behavior of bearings when various faults are developed in one of their parts throughout comparing the faulty conditions with the health condition. Figure 3. shows the four faulty bearings.

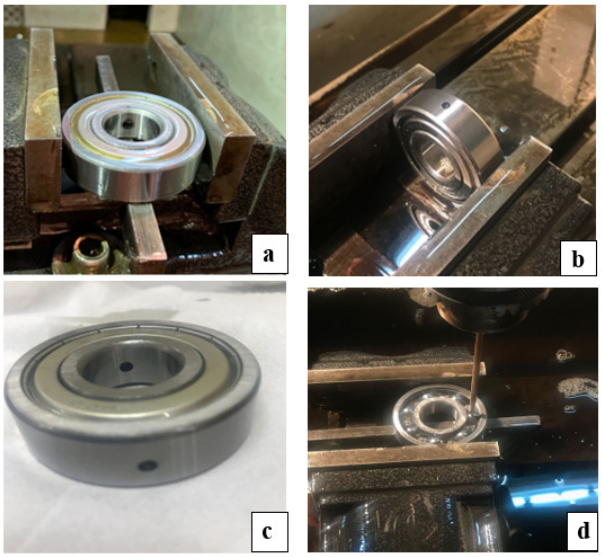


**Figure 3. Types of the simulated faults (a) Inner race fault (b) Outer race fault (c) Combined inner and outer race fault(d) Combined cage and ball**

**Table 2. The conducted experimental tests on the bearing**

| load | Healthy bearing | Inner race fault | Outer race fault | Combined cage and ball fault | Combined inner and outer race fault |
|---|---|---|---|---|---|
| 25Kg | 1000 RPM | | | | |
| | 1500 RPM | | | | |
| | 2000 RPM | | | | |
| 50Kg | 1000 RPM | | | | |
| | 1500 RPM | | | | |
| | 2000 RPM | | | | |

An increase in vibration amplitude occurs when the rolling element (ball) strikes the induced fault leading toa discontinuity in the emitted vibration signals. To

study the effect of these faults utilizing vibration analysis, the results from 30 conducted experiments on the developed test rig, considering various rotating speeds and different loading conditions, were investigated. The performed 30 test scenarios are shown in Table 2.

### 3.3 The Developed Data AcquisitionSystem

In order to monitor the working condition of the under investigation bearing, the vibration signals have to be captured and analyzed to find out if there is something abnormal in its health or not. Figure 4. shows the developed data acquisition system for vibration signal capturing using an accelerometer type ADXL335, which is a MEMS type sensor [34].

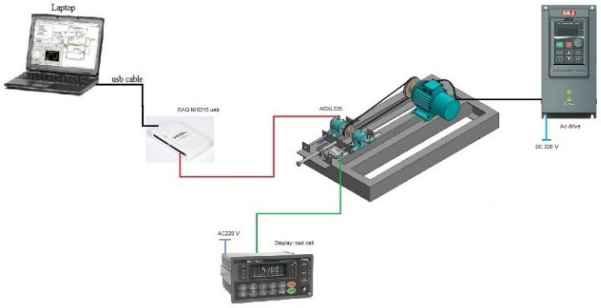


**Figure 4. A schematic diagram for the developed data acquisition system**

The obtained signals are then transferred to a computer that contains a developed LabView program, which analyses these signals and extracts the vital features from them. Finally, the applied load on the system can be measured using a load cell sensor connected directly to a Digital Panel Meter to display the amount of force.

### 3.4 Test rig operation

After installing the acceleration sensor on the monitored bearing, it is interfaced to the data acquisition system connected to the computer connected to the data acquisition. Next, the load cell is installed in its place, as shown in Figure 5. and connected to the digital panel meter that shows the tension readings directly and after running the electrical motor.

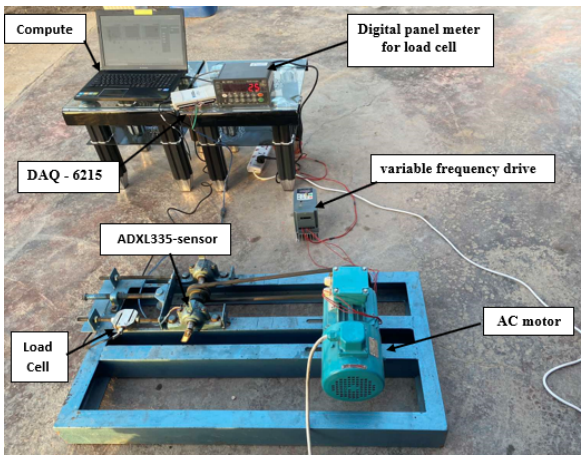


**Figure 5. Test rig final set-up**

The motor is connected to the AC drive, connected to the electrical socket, for speed variation. Finally, the device is started at the specified speed with fixed tension on the specified shaft. These steps are repeated when changing the simulated ball-bearing fault. The accelerometer readings are taken continuously using the developed LabVIEW program.

## 4. RESULTS AND DISCUSSION

Vibration signal analysis represents an effective technique that can be used for load variation and fault detection. However, in this study, five different bearing health states (healthy, inner race fault, outer race fault, combined inner and outer fault, and combined cage and ball fault) have been considered. Vibration signal capturing was conducted utilizing the developed data acquisition. Nevertheless, before data capturing when bearing fault was presented, the test rig was run for a short time to permit the rotating system to settle dynamically. Different time domain features were then calculated based on the theoretical equations that were discussed in section two. In the experimental work, the developed test rig was run at different operation/health conditions. The sampling frequency was taken equal to 1500 *Hz,* and the acquired number of samples was 500 samples. Two thousand five hundred thousand samples of the time-domain signal were taken at each experiment. After that, the captured time-domain signals are analyzed, then different features were extracted, and the important ones were selected. Based on the most significant selected features, the control charts are designed and then tested.Figure 6.shows the followed main steps in this research for bearing fault detection.

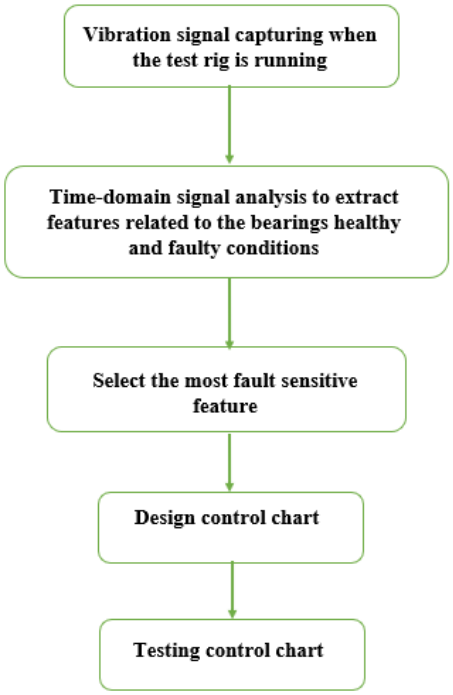


**Figure 6. Flowchart depicting the proposed stage of fault detection**

### 4.1 Captured vibration signals

To investigate the effect of loading conditions on the vibration signal variation when the bearing is healthy and then faulty (inner, outer race, combined inner and

outer, and ball and cage faults), the test rig was operated at a fixed rotating speed while the applied load is increased gradually. The captured signals are presented in Figure 7, which shows a slight increase in the vibration amplitude when increasing the applied load.

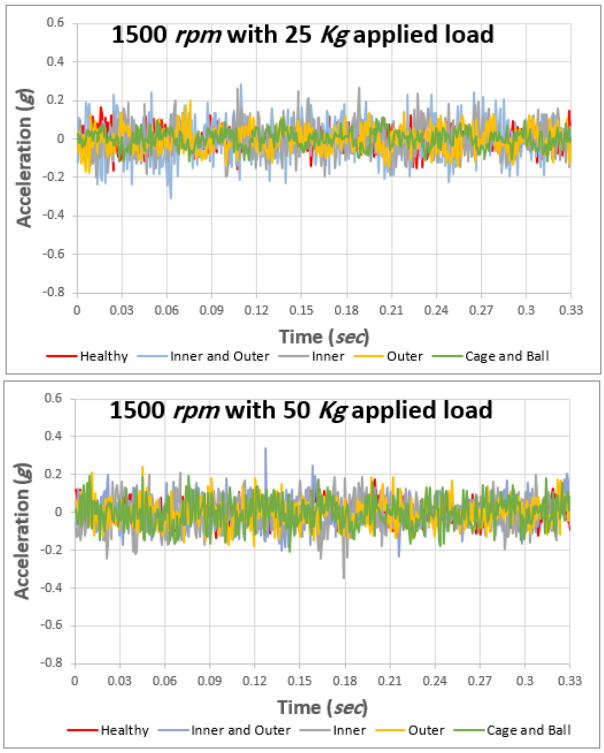


**Figure 7. Time-domain signals of the five bearing's health states at 1500 rpm with different applied loads**

The reason is that the increase in applied load puts a load on the system, causing load on the bearing, which leads to an increase in vibration amplitude. As a result, the combined fault (ball and cage) is highly affected than the other types of faults. It may be because the ball and cage fault leads to a higher vibration amplitude, and thus this type of damages is more dangerous than the other types.

### 4.2 Feature extraction

This section will analyze and discuss the effect of different loading conditions and extract statistical feature sets from the captured time-domain signals previously obtained from the experimental work. However, in order to choose the most fault-sensitive feature and use it later in designing the control chart, the root mean square (RMS), standard deviation (SD), kurtosis ($K_v$), skewness (Sk), and crest factor ($C_{rf}$) were extracted for each loading condition and in the healthy state and compared with the features of the faulty state, as shown in the following figures.

Figure 8. to Figure 12.show the values of RMS, SD, $C_{rf}$, $K_v$ and $Sk$ for the captured current signal after being divided into sub-signals. In these figures, the X-axis represents the order of the data sample (sample no.), and Y-axis represents their values. However, these figures can be noted that the calculated time domain features are altered as the difference occurred in the operation condition, such as changing the speed or the load. Furthermore, the amplitudes of the features are less when the bearing is healthy, while when the faults are simulated, the amplitudes get greater. This is because, in the presence of a fault, the vibration level becomes significant as when the inner race is rotated with the shaft, the ball collides with the simulated damage and thus produces high vibration amplitudes. It is also observed that the combined fault case (ball and cage) is more sensitive than other defects.

Figure 8 shows that when the applied load is increased for the same rotation speed, the RMS amplitude increases due to the existence of the faults. This can be attributed to the fact that as the fault severity increases, the vibration amplitude increases. This increase becomes higher as the applied load increases; this leads to an increase in the signal's energy content, indicated by the RMS values. However, the significant increase in the RMS values is in the case of combined fault.

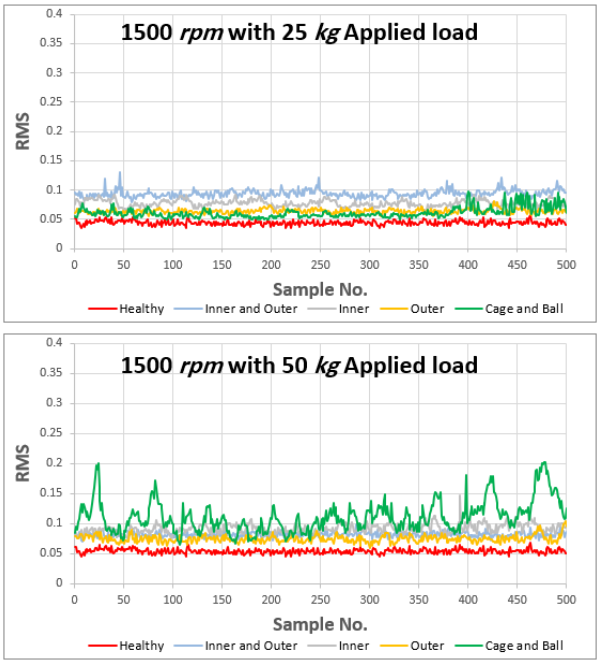


**Figure 8. Variation of RMS with the applied load**

Figure 9 indicates an increase in the values of the standard deviation feature for both healthy and faulty bearings as the applied load increases with the fixed rotation speed. Also, the combined fault case shows the highest standard deviation values than others.

In Figure 10, it can be observed that the kurtosis values give a clear indication of the fault intensity. The highest kurtosis values can be noticed for the combined fault cases in both loading conditions while the other fault cases come after. However, the kurtosis values for the healthy case are about three, which correctly indicating the system is healthy, as reported in many references [17].

Skewness is a statistical indicator of asymmetry in which the curve develops in a skewed manner. The graph can be skewed on one hand or the other. The value of skewness can be both positive and negative [1]. In terms of the skewness values that are depicted in Figure 11, it can be observed that the skewness patterns for the five bearing health states are overlapping, and there is not any useful information that can be gained

from them. Therefore, it can be concluded that the skewness feature is not highly affected by fault; thus, it can be ignored.

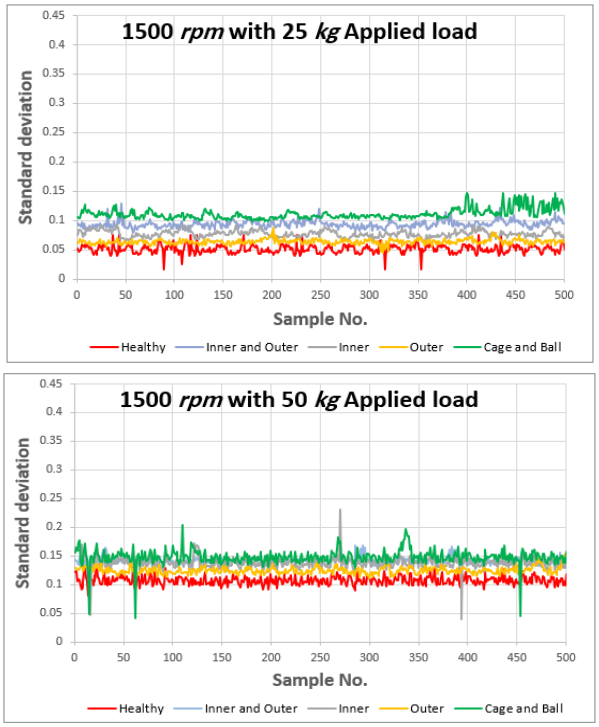


**Figure 9. Variation of standard deviation with the applied load**

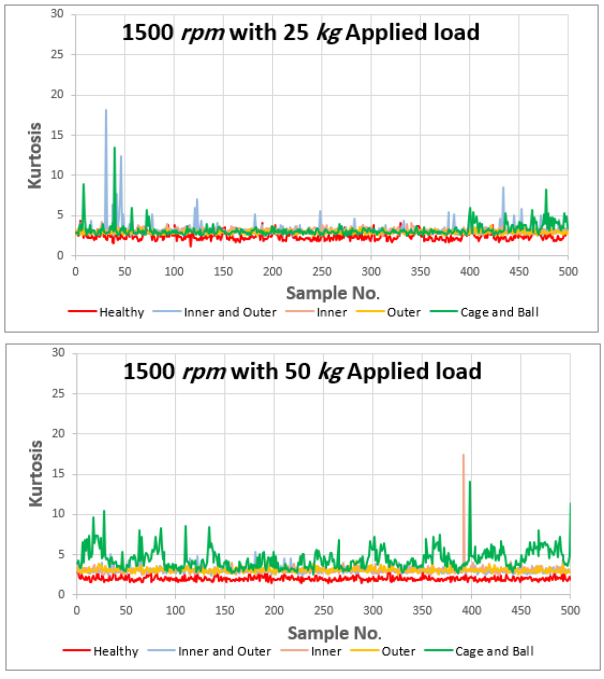


**Figure 10. Variation of kurtosis with applied load**

Figure 12 shows fast changes in the crest factor values for the different bearing health conditions. Hence, it decreases when the applied load increases. This can be attributed to an increase in the RMS values and a decrease in the peak values used to calculate the crest factor where the peak is in the numerator, and RMS is in the denominator, as mentioned previouslyin Equation 5.As a result, the crest factor is the highest in the combined fault cases in both loading conditions.

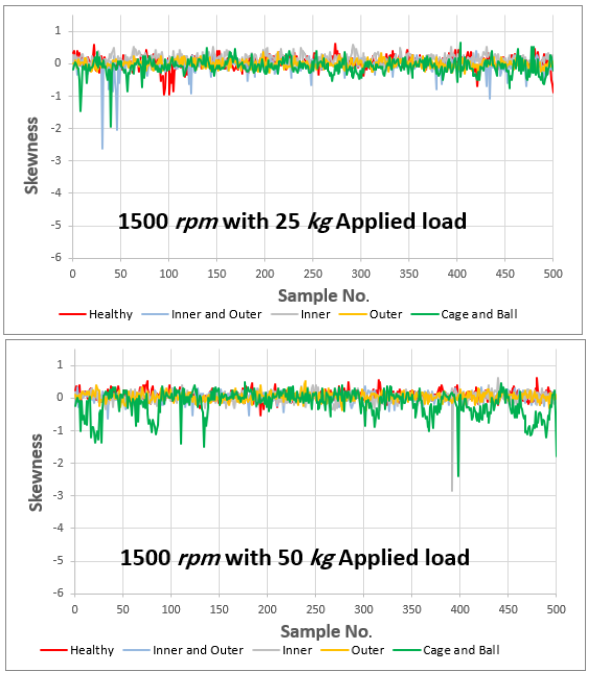


**Figure 11. Variation of skewness with applied load**

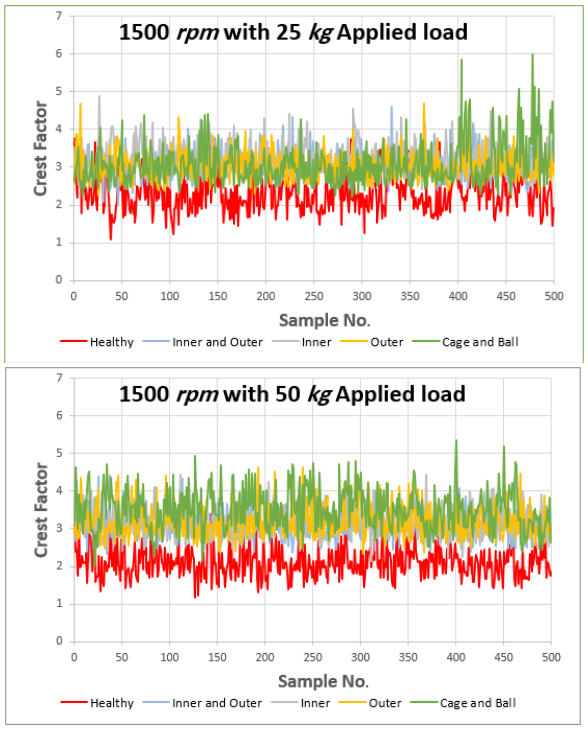


**Figure 12. Variation of Crest Factor with Applied Load**

In general, time-domain statistical features can represent mechanical health conditions from various perspectives since they can compensate for each other. On the other hand, each indicator can contain fault information in various fault harshness levels even though many features will mimic the changes in faults to some degree. As a result, it is recommended that more features be computed to diagnose rotating machinery faults effectively.However, time-domain signal analysis of vibration signals has limitations in terms of sensitivity and fault prediction accuracy. Therefore, combining the time domain features with the statistical control chart will improve the accuracy of monitoring and detecting faults at their early stages [3].

### 4.3 Feature selection

To design an appropriate control chart, a suitable feature that easily clarifies the machine's health condition must be selected. However, after analyzing the five obtained features from the time-domain signals, it was observed that the standard deviation feature is the most sensitive one. It clearly signifies the occurrence of faults at the different loading conditions. Thus, it is chosen to design the control chart and then analyze and test its capability for bearing fault detection.

### 4.4 Control chart design using CUSUM tabular method

The control chart is designed based on the standard deviation feature of the health-bearing case using Minitab software. For each of the previously considered operation speeds, a control chart has been designed. The obtained standard deviation data set is taken to the Minitab program to calculate their standard deviation and the target value, equal to the mean of the standard deviation values. In order to design the limits of the control chart, the constant of Equation 10 was chosen equal to 5 multiplied by the value of the standard deviation [29-31].

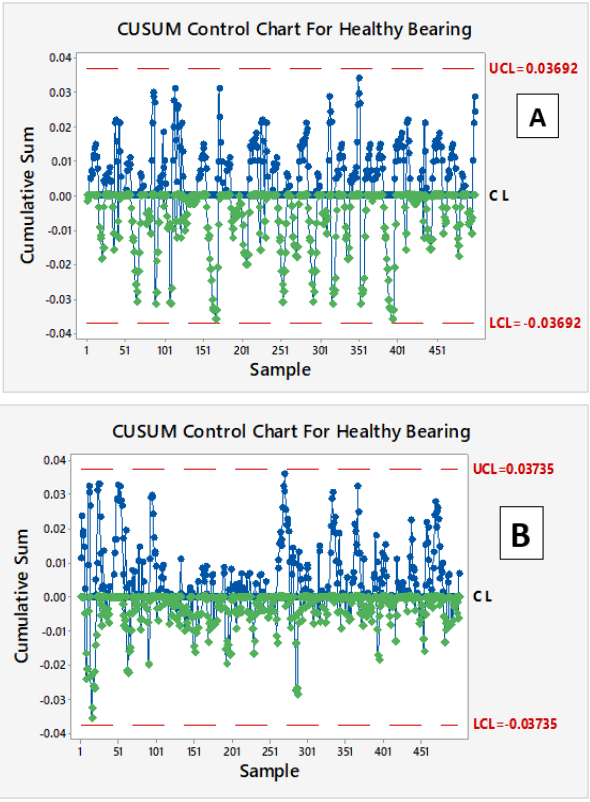


**Figure 13. CUSUM control chart for healthy bearing: (A) 1500 rpm with 25 Kg applied load (B) 1500 rpm with 50 Kg applied load**

The software draws the chart after taking the required information, as shown in Figure 13. First, it draws upper one-sided CUSUM represented by the blue color and lower one-sided CUSUM represented by the green color. Then, another three important lines are drawn, represented by two dashed red lines, which indicate the control chart's limits, and a central black line indicating the target line. In Figure 13, it can be noticed that all points of the healthy state are lying between the upper control limit (UCL) and lower control limit (LCL), indicating that the bearing is healthy and not out of control. However, it can be noticed that the control limits are increased as the rotating speed increased when the applied load is constant. Also, the same happens when the applied load increases at a constant rotating speed. This is because the amplitude of the standard deviation increases when the load conditions are increased. Hence, this chart can help technicians in charge of machine health monitoring easily identify if the bearing is under control or not at different operating conditions.

### 4.5 Control Chart Testing

As discussed previously, to detect the faults at their early stages to avoid catastrophic damages and verify if the designed control chart works properly or not, the same feature used in designing the control chart is used to test it. The standard deviation features extracted from the vibration signals of bearing with different fault types are utilized in this step. The faults include the inner race fault, outer race fault, and combined faults. The standard deviation features for each fault condition are transferred to the Minitab program, enter the target that which equals the mean for the readings taken and enter the standard deviation of the total readings of the healthy status state that were designed for the same rotation speed and load applied on the faulty. This step is repeated every time to test all defective health conditions taken in proven conditions.It is considered that the system is under control if all the taken and drawn standard deviation features are within the control limits. However, it was noted that all the considered readings were lying within the control limits for healthy bearing.

Figures 14 and 15show that the process is out of control due to the appearance of some points that cross the allowed control limits, which are expressed by the red color. However, in the case of inner race defect and combined cage and ball defect, the out-of-control points' values decrease as the rotation speed increases with constant applied load and vice versa. This is due to when the speed increases, the value of control limits increases too. On the other hand, in the case of the outer race defect and the combined inner and outer race defect, the number of points emerging from the control limits increased as the rotation speed increased with constant applied load and vise versa.

Figures 14 and 15 for the combined cage and ball fault show that this fault is one of the most out-of-control cases, and the defect can be easily detected. Where it was found that the ratio of the peaks that were calculated at rotation speed 1500 rpm and applied load 25 kg between the cumulative sum control chart for the combined defect of the ball and the cage from the peak of the fault in the case of the inner race is equal to 72.6% and its ratio to the peak of the outer race fault is equal to 85.6% and also its ratio for the inner and outer compound defect is equal to 80.1%. The reason can be attributed to that if the inner or outer race fault (or both are faulty), the ball will hit the made defect every time it passes over it. However, when

the ball itself is defected and also the cage, this means a complete bearing failure because the defect in the ball during the entire rotation period is hitting the inner and outer races of the bearing, leading to increasing the feature amplitude and hence significantly increasing the upper and lower cumulative sum in the control chart. Thus, the bearing damage is considered very severe; therefore, it can be easily identified.

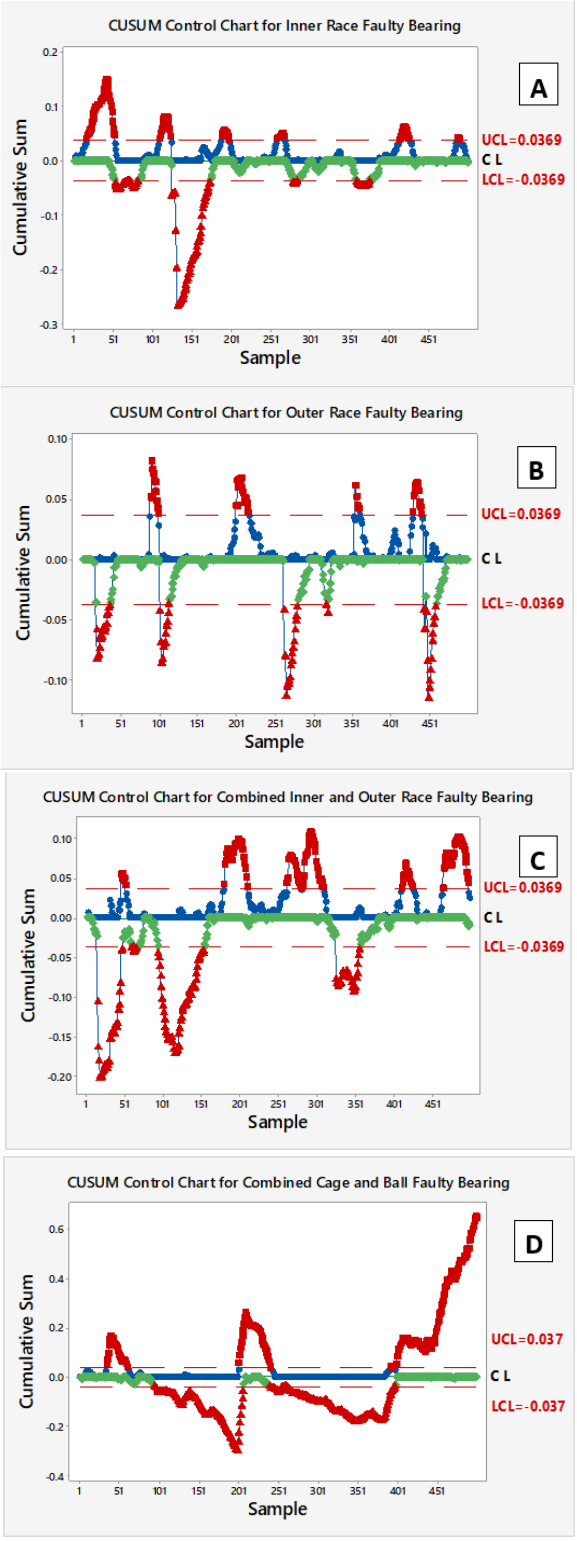


**Figure 14. CUSUM control chart for faulty bearing at 1500 rpm and 25 Kg applied load: (A) inner race faulty (B) outer race faulty (C) inner and outer race faulty (D) cage and ball faulty.**

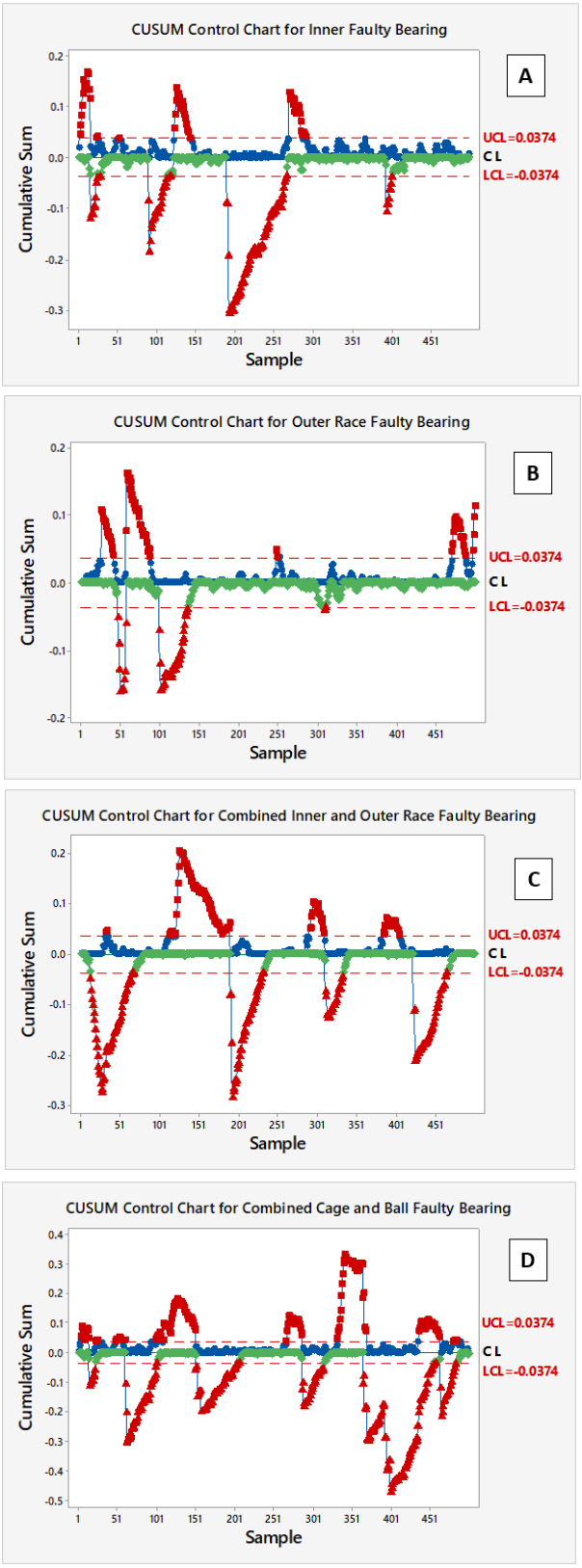


**Figure 15. CUSUM control chart for faulty bearing at 1500 rpm and 50 Kg applied load: (A) inner race faulty (B) outer race faulty (C) inner and outer race faulty (D) cage and ball faulty**

It can be noticed in Figure 15 that the out-of-control points due to the inner race defect (A) are having higher amplitudes than the points that are related to the outer race defect. The reason for this is that although the size of the inner raceis smaller than the size of the outer race, the

inner race always rotates with the shaft meaning that the defect is continuously hitting the balls. Thus, its vibration amplitude will be higher, so the feature's amplitudes increase, increasing the upper cumulative sum. Nevertheless, when the combined inner and outer race fault happens, the number of points that are out of control will be more because it contains two faults at the same time.

## 5. CONCLUSION

In this research, a fault detection system for bearings was developed based on features extracted from the time-domain vibration signals and the statistical control chart approach. An experimental test rig was designed and fabricated to accomplish the experimental part of this work. Different experiments were carried out to investigate the effect of different bearings' health states on the machines' vibration severity. The simulated bearing faults included inner race fault, outer race fault, combined inner and outer race fault, and combine ball and cage fault. Vibration signals were captured utilizing a data acquisition system developed based on National Instrument hardware (NI 6215 DQA) and software (LabVIEW). The vibration signals were captured at different applied loads when different faults were embedded in the bearing. However, based on the experimental findings, the following conclusions can be drawn:

1. Vibration-based condition monitoring and statistic control chart can effectively detect the bearing faults by monitoring the extracted time-domain features from the captured vibration signals.

2. The influence of a bearing fault is varying depending on the applied load.

3. When the bearing is healthy, the amplitudes of the features are small, while when faults are simulated, the amplitudes increase. When the inner race rotates with the shaft, the ball will always hit the simulated damage and causes high vibration amplitudes; the vibration level becomes more significant as the fault gets severer.

4. It can be inferred that the combined defects (inner and outer race fault and cage and ball fault) are more severe, more sensitive to applied load and rotation speed, and have a greater impact on the overall vibration level of the rotating system. This can be attributed to the fact that the combined fault case involves two faults simul–tane–ously, which produces the highest vibration amplitudes. As a result, the induced vibration level increases and becomes extreme with increasing applied load.

5. The combined ball and cage fault was often found to be more sensitive than other fault types, which means that the ball or cage defect refers to faster bearing damage than other faults.

6. The extracted time domain features from vibration signals, such as root mean square, kurtosis, and Crest factor, clearly indicate the bearing's health condition.

7. The CUSUM control chart is an effective technique for detecting various small sizes bearing faults using features selected from time-domain vibration signals.

8. Signal analysis using the time-domain signal ana–lysis technique can extract features related to simulated faults. It is often considered a simple signal analysis technique and can be more effective when combined with the control chart.

## REFERENCES


[1] A. A. Borhana, U. Shankar, R. Kalaivani, M. Khattak, Y. H. Ali, and O. S. Zaroog, "Early fault detection in bearing using time domain technique: faulty bearing seeded on inner raceway and ball."

[2] S. Fu, K. Liu, Y. Xu, and Y. Liu, "Rolling bearing diagnosing method based on time domain analysis and adaptive fuzzy-means clustering," *Shock and Vibration,* vol. 2016, 2016.

[3] O. P. Yadav and G. Pahuja, "Bearing health assessment using time domain analysis of vibration signal," *International Journal of Image, Graphics and Signal Processing,* vol. 12, p. 27, 2020.

[4] J. J. Saucedo-Dorantes, M. Delgado-Prieto, J. A. Ortega-Redondo, R. A. Osornio-Rios, and R. d. J. Romero-Troncoso, "Multiple-fault detection methodology based on vibration and current analysis applied to bearings in induction motors and gearboxes on the kinematic chain," *Shock and Vibration,* vol. 2016, 2016.

[5] S. Orhan, N. Aktürk, and V. Celik, "Vibration monitoring for defect diagnosis of rolling element bearings as a predictive maintenance tool: Comprehensive case studies," *Ndt & E International,* vol. 39, pp. 293-298, 2006.

[6] E. A. Khazem, O. I. Abdullah, and L. A. Sabri, "Steady-state and vibration analysis of a Wind-PACT 1.5-MW turbine blade," *FME Transactions,* vol. 47, pp. 195-201, 2019.

[7] Marwah.A.Husain and A. A.-s. Mohsin, "Effect of Cracks on the Natural Frequency of Cylindrical Shell Structures," *Engineering and Technology Journal* vol. 38, pp. 1808-1817, 2020.

[8] A. J. Kadhum, A. S. Mohamed, and S. A. Hayder, "Numerical Study of Effect of Using Nanofluids Flowing in Simply Supported Pipes on Vibrations Characteristics," *Engineering and Technology Journal* vol. 38, pp. 43-56, 2020.

[9] M. Cococcioni, B. Lazzerini, and S. L. Volpi, "Rolling element bearing fault classification using soft computing techniques," in *2009 IEEE International Conference on Systems, Man and Cybernetics*, 2009, pp. 4926-4931.

[10] S. Zhang, J. Mathew, L. Ma, Y. Sun, and A. Mathew, "Statistical condition monitoring based on vibration signals," *QUT Digital Repository:,* 2004.

[11] S. M. Jawad, A. A. Jaber, "A Data-Driven Approach Based Bearing Faults Detection and Diagnosis: A Review," in *IOP Conference Series: Materials Science and Engineering*, 2021, p. 012111.

[12] S. Patidar, P. K. Soni, "An overview on vibration analysis techniques for the diagnosis of rolling element bearing faults," *International Journal of*

*Engineering Trends and Technology (IJETT),* vol. 4, pp. 1804-1809, 2013.

[13] P. R. Manve, R. S., "Condition monitoring and fault identification of new deep groove ball bearing using LABVIEW," *Journal of Emerging Technologies and Innovative Research (JETIR),* vol. 4, 2017.

[14] B. Sreejith, A. Verma, and A. Srividya, "Fault diagnosis of rolling element bearing using time-domain features and neural networks," in *2008 IEEE Region 10 and the Third international Conference on Industrial and Information Systems*, 2008, pp. 1-6.

[15] S. Riaz, H. Elahi, K. Javaid, and T. Shahzad, "Vibration feature extraction and analysis for fault diagnosis of rotating machinery-a literature survey," *Asia Pacific Journal of Multidisciplinary Research,* vol. 5, pp. 103-110, 2017.

[16] S. Kulkarni and A. Bewoor, "Vibration based condition assessment of ball bearing with distributed defects," *Journal of Measurements in Engineering,* vol. 4, pp. 87-94, 2016.

[17] W. Caesarendra and T. Tjahjowidodo, "A Review of Feature Extraction Methods in Vibration-Based Condition Monitoring and Its Application for Degradation Trend Estimation of Low-Speed Slew Bearing," *Machines,* vol. 5, p. 21, 2017.

[18] H. Musbah and M. El-Hawary, "SARIMA Model Forecasting of Short-Term Electrical Load Data Augmented by Fast Fourier Transform Seasonality Detection," in *2019 IEEE Canadian Conference of Electrical and Computer Engineering (CCECE)*, 2019, pp. 1-4.

[19] R. Pidl and P. Böröcz, "Discrete fourier transform and cepstrum analysis of vibration events on semi-trailer truck," *FME Transactions,* vol. 47, pp. 177-182, 2019.

[20] P. Gupta and M. Pradhan, "Fault detection analysis in rolling element bearing: A review," *Materials Today: Proceedings,* vol. 4, pp. 2085-2094, 2017.

[21] Z. Xia, S. Xia, L. Wan, and S. Cai, "Spectral regression based fault feature extraction for bearing accelerometer sensor signals," *Sensors,* vol. 12, pp. 13694-13719, 2012.

[22] M. Riaz, N. Abbas, and R. J. Does, "Improving the performance of CUSUM charts," *Quality and Reliability Engineering International,* vol. 27, pp. 415-424, 2011.

[23] P. E. Maravelakis, "Measurement error effect on the CUSUM control chart," *Journal of Applied Statistics,* vol. 39, pp. 323-336, 2012.

[24] A. Haq, "A new hybrid exponentially weighted moving average control chart for monitoring process mean," *Quality and Reliability Engineering International,* vol. 29, pp. 1015-1025, 2013.

[25] A. Begun, E. Kulinskaya, and A. J. MacGregor, "Risk-adjusted CUSUM control charts for shared frailty survival models with application to hip replacement outcomes: a study using the NJR dataset," *BMC medical research methodology,* vol. 19, p. 217, 2019.

[26] E. M. S. Alamer, "CUSUM Control Charts for Censored Gamma Distributed Quality Measurements," 2017.

[27] M. Awais and A. Haq, "A new cumulative sum control chart for monitoring the process mean using varied L ranked set sampling," *Journal of Industrial and Production Engineering,* vol. 35, pp. 74-90, 2018.

[28] N. Abbas, M. Riaz, and R. J. Does, "Mixed exponentially weighted moving average–cumulative sum charts for process monitoring," *Quality and Reliability Engineering International,* vol. 29, pp. 345-356, 2013.

[29] D. Montgomery and G. Runger, "Applied Statistics and Probability for Engineers. New Jersey: John Wily and Sons," ed: Inc, 2018.

[30] D. C. Montgomery and G. C. Runger, *Applied statistics and probability for engineers*: John Wiley & Sons, 2010.

[31] B. Zaman, M. Riaz, N. Abbas, and R. J. Does, "Mixed cumulative sum–exponentially weighted moving average control charts: an efficient way of monitoring process location," *Quality and Reliability Engineering International,* vol. 31, pp. 1407-1421, 2015.

[32] A. A. Jaber and K. M. Ali, "Artificial neural network based fault diagnosis of a pulley-belt rotating system," *International Journal on Advanced Science, Engineering and Information Technology,* vol. 9, pp. 544-551, 2019.

[33] A. A. Jaber and R. Bicker, "Fault diagnosis of industrial robot bearings based on discrete wavelet transform and artificial neural network," *International Journal of Prognostics and Health Management,* vol. 7, 2016.

[34] F. M. Nasheed, F. S. Waleed, and F. S. Faez, "Design of Oil Pipeline Monitoring System based on Wireless Sensor Network," *IRAQI JOURNAL OF COMPUTERS, COMMUNICATION, CONTROL & SYSTEMS ENGINEERING* vol. 18, pp. 53-62, 2018.

## NOMENCLATURE

| | |
|---|---|
| $P_v$ | Peak value |
| RMS | Root Mean Square |
| SD | Standard Deviation |
| $K_v$ | Kurtois Value |
| $C_{rf}$ | Crest Factor |
| Sk | Skewness |
| $S_H$(i) | Upper One-Sided Cusum |
| $S_L$(i) | Lower One-Sided Cusum |
| K | Reference Value |
| UCL | Upper Control Limit |
| LCL | Lower Control Limit |

***Superscripts***

| | |
|---|---|
| *EWMA* | Exponentially Weighted Moving Average |

| | |
|---|---|
| *CUSUM* | Cumulative Sum |
| *S* | Standard Deviation Chart |
| R | Range Chart |
| FFT | Fast Fourier Transform |
| STFT | Short-Time Fourier Transform |
| WT | Wavelet Transform |
| WPT | Wavelet Packet Transform |
| HHT | Hilbert-Huang Transform |
| EMD | Electrical Discharge Machining |

## ДЕТЕКЦИЈА ОТКАЗА КОТРЉАЈНИХ ЛЕЖАЈЕВА ПРИМЕНОМ АНАЛИЗЕ СИГНАЛА ВИБРАЦИЈА И КОНТРОЛНЕ КАРТЕ КУМУЛАТИВНИХ СУМА

**С.М. Џавад, А.А. Џабер**

Праћење стања ротационих машина је од значаја за безбедност система, смањење трошкова одржавања и повећање поузданости. У раду је развијен систем за детекцију отказа лежајева применом технике анализе вибрација са CUSUM дијаграмом. Прво је дизајнирана и израђена тест опрема а потом је извршена симулација и испитивање различитих отказа лежајева као нпр. отказа унутрашњег и спољашњег жлебног прстена. После снимања сигнала вибрација у различитим условима испра–вности лежајева, издвојене су различите индика–тивне карактеристике помоћу анализе сигнала у временском домену. Добијене карактеристике су анализиране да би се добила најзначајнија карактеристика – отказ. Затим је одабрана само једна карактеристика на основу које је дизајнирана контролна карта за праћење стања исправности лежаја. CUSUM дијаграм је коришћен, јер може да детектује мале промене стања исправног рада лежајева. Резултати су показали ефикасност метода и утврђено је да је проценат грешке ван контроле у случају комбинованог отказа кавеза и куглице у односу на број испитаних узорака већи него код осталих типова отказа.